Final Project: A DFT Verification of K-point Instabilities of the γ'-Fe_4N Crystal Structure

Lórien MacEnulty,* Andrew Burgess,† and David Gavin‡
Trinity College Dublin
2 College Green, Dublin 2, Ireland

(Group 4: The LADs)
(Dated: December 5, 2020)

We verify and reinspect those density functional theory results heralded in Cheng *et al* on the response of the γ'-Fe_4N crystal structure to increasing pressure. By converging our parameters with respect to the hydrostatic pressure, we found our converged k-point mesh, wavefunction energy cutoff and charge density energy cutoff to be 9x9x9, 151 Ry and 604 Ry respectively. This k-point mesh is similar to the one employed by Cheng *et al* (10x10x10), however our cut-off energies are much higher. Using the converged parameters we found the E(V)-curve for γ'-Fe_4N and used this to find the equilibrium volume of 54.62 Å^3 and a bulk modulus of 166.2 GPa. At 10 GPa the volume of the γ'-Fe_4N unit cell decreased by $5.37\% - 6.89\%$ in slight disagreement with the value found by Cheng *et al* (6.98%) and at 30 GPa we found that the volume decreased by (14.22%). The soft mode procedure was used to predict the existence of the low-symmetry P1m1-Fe_4N structure, which was shown to have lower total energy than γ'-Fe_4N at 30 GPa. The P2/m structure of Fe_4N was shown to be more stable than both γ'-Fe_4N and our newly found P1m1-Fe_4N for pressures greater than 4 GPa. It is possible that there exists a more stable phase of Fe_4N at 30 GPa that is consistent with a displacive distortion on a non-linear supercell that wasn't investigated here.

Keywords: *DFT, applied computational mathematics, Ghent University Course, Steffan Cottenier*

I. INTRODUCTION

The magnetic, catalytic and chemical properties of γ'-Fe_4N has sustained considerable research interest since the 1930s when it was investigated for the Haber-Bosch process.[1] Current work focuses on its use as an inexpensive electrocatalyst for water oxidation.[2] An interstitial compound, γ'-Fe_4N forms a face-centred cubic γ-Fe structure with nitrogen atoms in the body centered octahedral holes.[3] It crystallizes in the $Pm\bar{3}m$ space group, with Fe at the 1a (0,0,0) and 3c (0.5, 0, 0.5) sites and N at the 1b (0.5, 0.5, 0.5) site.[4]

γ'-Fe_4N is a strong ferromagnet, with a curie temperature T_C of 769 K and low temperature magnetic moment of 8.8 μ_B per formula unit.[4] Hybridization of the N *sp* states with the nearest neighbour Fe *d* states lowers the potential experienced by the 3d $\downarrow$-spin electrons. This leads to significant charge transfer from the 1a to the 3c Fe sites, mostly of $3d\downarrow$ character.[5] This in turn results in a higher magnetic moment on the 1a site (2.98 μ_B) than the 3c site (2.01 μ_B).[5]

Recent density functional theory (DFT) studies of Fe_4N by Cheng *et al* report a new, dynamically stable phase for Fe_4N in the P2/m space group.[4] Cheng *et al* observed a soft mode phase transition of γ'-Fe_4N ($Pm\bar{3}m$) at 10 GPa, with a softening of the acoustic phonons at the M point (0.5, 0.5, 0), i.e. the acoustic phonon frequencies ω become imaginary at the M point ($\omega^2 < 0$) [6]. The P2/m-Fe_4N phase is less symmetric than the cubic $Pm\bar{3}m$ crystal structure, with Cheng *et al* reporting lattice constants of 5.24780, 5.24780 and 3.71980 Å at 10 GPa.[4]

II. TASK 1: PARAMETER CONVERGENCE TESTING

Using a DFT code rising in popularity, QUANTUM ESPRESSO, as opposed to the VASP infrastructure employed by Cheng *et al*, we embarked on computational verification.[7] We used the PBE exchange correlation

kmesh	HS Pressure (kbar)	CPU time
1x1x1	43.24	2m12
2x2x2	-9.08	3m41
3x3x3	-35.95	3m21
4x4x4	-48.92	5m39
5x5x5	-39.37	5m40
6x6x6	-44.83	9m33
7x7x7	-43.09	9m38
8x8x8	-46.93	15m28
9x9x9	-46.68	15m34
10x10x10	-34.13	25m13
11x11x11	-36.65	23m34

FIG. 1: k-mesh density convergence. We decided on a k-mesh of 9x9x9, a suitable compromise between precision and CPU time.

* lmacenul@tcd.ie
† burgesan@tcd.ie
‡ gavind3@tcd.ie

functional and projected augmented wave (PAW) pseudopotentials to perform spin-polarized self-consistent field calculations on the $Pm\bar{3}m$ Fe_4N system at ground state using the lattice parameter reported in Table 2 of the model paper ($a = 3.795$Å). The unit cell was taken to be standard cubic, and the relaxation of atoms adopted a Methfessel-Paxton smearing method (smearing width of 0.2 eV). Electrons were considered relaxed after a threshold precision of $1.0 * 10^{-6}$ was reached.

To begin, we converged our parameters with respect to the reported hydrostatic pressure, a value known to be highly sensitive to DFT parameter choice, to achieve suitable precision of our results as a function of runtime. Notable parameters are the k-mesh density, the energy cutoff and the density cutoff (denoted, respectively, k-points, ecutwfc and ecutrho in the QUANTUM ESPRESSO terminology). The results of this convergence testing are found in Figures 1-3.

ecutwfc (Ry)	ecutrho (Ry)	HS Pressure (kbar)	CPU time
51	357	-145.06	46.09
61	427	-20.78	49.77
71	497	-42.98	53.01
81	567	-28.6	57.52
91	637	-9.11	1m0.29
101	707	-3.95	1m3.62
111	777	-6.26	1m7.43
121	847	-7.68	1m10.92
131	917	-6.55	1m14.54
141	987	-4.57	1m31.45
151	1057	-3.32	1m35.23
161	1127	-3.65	1m43.05
171	1197	-4.22	1m43.63
181	1267	-4.42	1m51.41
191	1337	-4.03	2m0.65

FIG. 2: ecutwfc convergence testing. Keeping ecutrho = 7*ecutwfc, we decided on $ecutwfc = 151$ because it was a nice compromise between precision and CPU time. NOTE: Here, we used a different computer, which is why the times are so much faster.

factor	ecutrho (Ry)	HS Pressure (kbar)	CPU time
2	302	-7.07	28.51
3	453	-8.18	42m15
4	604	-8.51	57m55
5	755	-8.51	58m35
6	906	-8.49	59m3
7	1057	-8.29	59m54
8	1208	-8.33	1h0m
9	1359	-8.31	1h0m

FIG. 3: ecutrho convergence. Keeping $ecutwfc = 151$ Ry and the k-mesh density at 9x9x9 while altering ecutrho as an integral multiple (denoted by factor) of ecutwfc.

After some trouble, we settled on a k-mesh density of 9x9x9, an ecutwfc of 151 Ry, and an ecutrho of 604 Ry (a value four times that of ecutwfc). See table captions for more details. For comparison, Cheng *et al* used a k-mesh density of 10x10x10 and a cutoff energy of 800 eV. Our converged values are much higher than those reported in the paper, which could be an artefact of the differing DFT infrastructures or possibly a higher convergence threshold. Regardless, our hydrostatic pressure is converged to within 0.5 kbar, which is satisfactory for our purposes.

III. TASK 2: ENERGY VS. VOLUME CURVE

Once parameters were sufficiently converged, we tested the total energy of the $Pm\bar{3}m$ γ'-Fe_4N crystal structure as a function of volume and by extent, because of the cubic symmetry intrinsic to the unit cell, as a function of lattice parameter a. The results of such calculations are found in Figure 5. The corresponding Energy vs. volume plot is found in Figure 4.

A Birch-Murnaghan equation was fitted to the data and a minimal χ^2 correlation value of $0.7102 * 10^{-7}$ obtained. This fit yielded an equilibrium volume of $V_0 = 54.62$Å^3, which corresponds to an equilibrium lattice parameter of $a_0 = 3.794$Å. This lattice parameter is very close (i.e., within 0.03%) to that used by Cheng *et al*, which was $a_0 = 3.795$Å. The BM fit also determined a bulk modulus for the crystal of 166.2 GPa.

Of the insights garnered from Figure 4, we note that a pressure of approximately 10 GPa was achieved when the lattice parameter was between 3.705 Å and 3.725 Å. At these pressures, the volume of the crystal has reduced by a value between 5.37% and 6.89%. This window disagrees slightly with the value provided by Cheng *et al*, which reported a pressure of 10 GPa obtained when

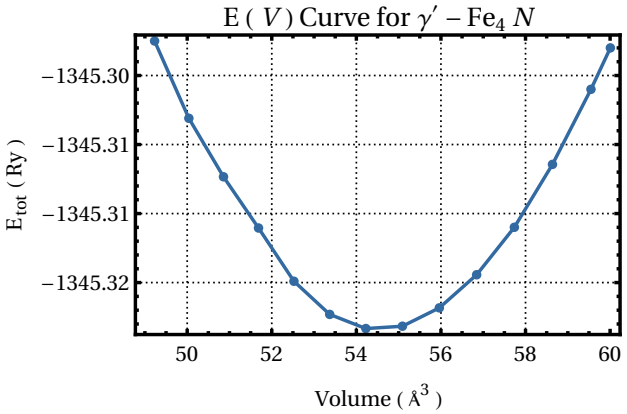

FIG. 4: The E(V) curve for γ'-Fe_4N. The Birch-Murnaghan fit was made for data between +/- 10% of equilibrium volume to ensure reliability. Data points in Figure 4.

$a = 3.70463$ Å; in their case, the volume at that pressure decreased by 6.98%.

We also draw the reader's attention to $a = 3.605$ Å, which ensured obtainment of a pressure of 30.03 GPa. At this pressure, the volume of the crystal has reduced by about 14.22%.

a(Å)	V(Å^3)	$E_{tot}(Ry)$	Pressure (GPa)
3.445	40.89	-1345.112	93.19
3.465	41.60	-1345.141	83.50
3.485	42.33	-1345.167	74.79
3.505	43.06	-1345.191	65.26
3.525	43.80	-1345.212	57.42
3.545	44.55	-1345.230	49.55
3.565	45.31	-1345.246	42.12
3.585	46.08	-1345.260	35.56
3.605	46.85	-1345.272	30.03
3.625	47.63	-1345.282	25.58
3.645	48.43	-1345.291	21.00
3.665	49.23	-1345.298	17.20
3.685	50.04	-1345.303	13.58
3.705	50.86	-1345.308	9.94
3.725	51.69	-1345.311	9.36
3.745	52.52	-1345.314	7.35
3.765	53.37	-1345.317	4.09
3.785	54.22	-1345.318	0.81
3.805	55.09	-1345.318	-1.07
3.825	55.96	-1345.316	-4.04
3.845	56.84	-1345.314	-7.16
3.865	57.74	-1345.311	-9.94
3.885	58.64	-1345.306	-11.55
3.905	59.55	-1345.301	-15.06
3.915	60.01	-1345.298	-14.58

FIG. 5: Total energy as reported by Quantum Espresso DFT calculations as a function of volume V and, by extent, lattice parameter a. The volume corresponding to the minimized energy was found to be 54.62Å^3.

IV. TASK 3: THE M-INSTABILITY

The thermodynamic stability of the low symmetry P2/m-Fe_4N was investigated from 0 to 40 GPa by executing a full geometry optimization at each increment of pressure. A pressure convergence threshold of 0.05 GPa was set. The initial internal coordinates and lattice parameters for the spin polarized DFT calculations were taken from Cheng *etal* first principles study of P2/m-Fe_4N.[4]

V. TASK 4: THE X-INSTABILITY

Figure 6 of the paper by Cheng *et al* reports the phonon spectrum of γ'-Fe_4N under a pressure of 30 GPa. Similar to the 10 GPa case, we can see the existence off a soft mode (negative frequency) in the phonon spectrum, this time occuring at the X-point (0, 0.5, 0). The atomic displacements associated with a soft mode are time-independent and are therefore permanent. As a result, a mechanism is provided for a phase transition to a new crystal structure, known as a displacive phase transition.[8]

In order to find suitable candidate structures for this new phase, we apply displacive distortions that are compatible with the X-phonon to the original high-symmetry γ'-Fe_4N structure. This procedure is carried out using the ISODISTORT tool.[9, 10] Using this tool, we investigated the effects of the X5-C1 distortion on the 1x2x1 supercell of γ'-Fe_4N. The X5-C1 distortions include a phonon, with five degrees of freedom and three strains, one of which has two degrees of freedom.

Displacive distortions resulting from the X5-C1

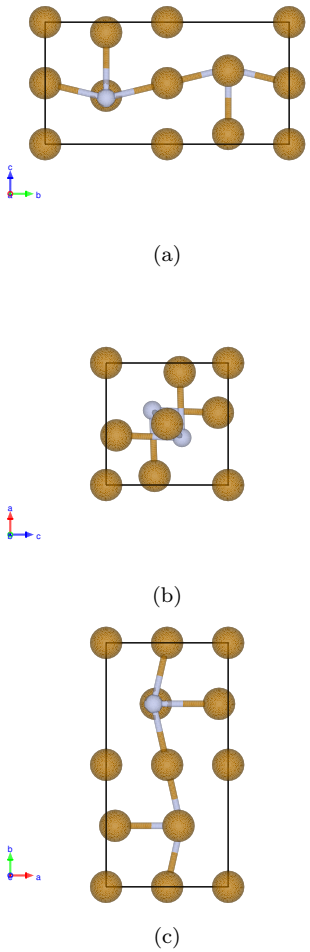

(a)

(b)

(c)

FIG. 6: Displacive distortions resulting from the X5-C1 phonon applied to the 1x2x1 supercell of γ'-Fe_4N. A large amplitude of the distortion is used here for ease of visualization, whereas a smaller amplitude would be more realistic for use in DFT calculations.

phonon can be seen in Figure 6. Large amplitudes (~ 0.8) were used for the displacements seen in Figure 6 so that they were easily visible. Smaller amplitudes (~ 0.2), however, are more realistic for use in DFT calculations. While the phonon distortions change the position of the atoms within the cell, the strains act to change the shape of the cell. Out of the three strains present here, they produced a uniform cell expansion, a tetragonal deformation and a monoclinic deformation respectively. Consequently, we combined the results of the phonon distortion and the strain, which produced the monoclinic deformation to create the most general .cif file compatible with the X5-C1 distortion. This new low-symmetry structure is in the P1m1 space group.

Geometry optimization was then performed on the aforementioned P1m1 structure with initial parameters $a = c = 3.8148$, $b = 7.55846$, $\alpha = \gamma = 90.0°$, $\beta = 89.82°$ and internal atomic positions in agreement with those seen in Figure 6 but with reduced distortion amplitude. The resulting relaxed structure had internal atomic positions which agreed with the γ'-Fe_4N structure to three significant figures and the c/a ratio reverted back to two, however the structure remained slightly monoclinic with $\beta = 89.9726°$.

The E(V)-curve of this new P1m1 structure was then determined by performing geometry relaxations at pressure values in the 0-40 GPa range, in line with the procedure carried out in Task 3. The resulting E(V)-curve can be seen in Figure 7.

Examining Figure 7, we see that P1m1-Fe_4N has a lower total energy than γ'-Fe_4N at 30 GPa, which was anticipated, however, there is only a marginal difference. P1m1-Fe_4N and P2/m-Fe_4N appear to have very similar total energies at 30 GPa. The enthalpies of P1m1-Fe_4N and P2/m-Fe_4N at 30 GPa are -1344.6279 Ry and -1344.6283 Ry respectively, indicating that P2/m-Fe_4N is slightly more thermodynamically stable at 30 GPa. Furthermore, it is evident that P2/m-Fe_4N is also more energetically favourable for pressures greater than 30 GPa.

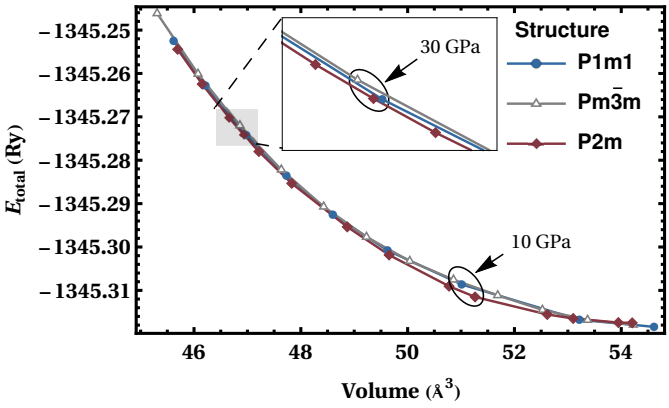

FIG. 7: The E(V)-curves per formula unit of the three different structures of Fe_4N that were treated in this investigation. This indicates which structures are the most stable for a given pressure or volume.

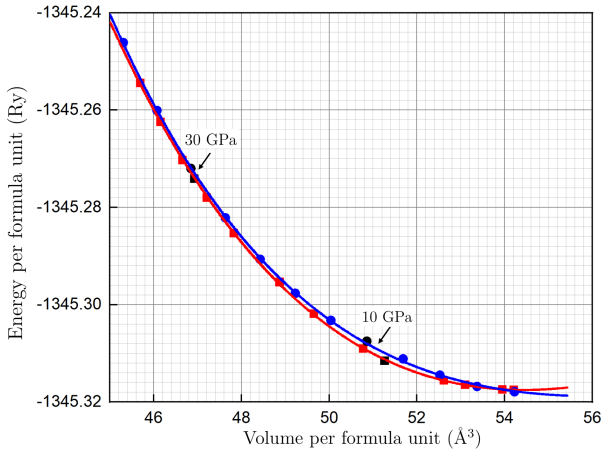

FIG. 8: Energy versus volume curve for Pm$\bar{3}$m-Fe_4N (blue circles) and P2/m-Fe_4N (red squares), between 0 and 43 GPa. Both energy (in Ryberg) and volume (in Å^3) are given per formula unit. The Pm$\bar{3}$m-Fe_4N and P2/m-Fe_4N volumes at 10 GPa and 30 GPa are highlighted in black and labelled on the graph.

We also performed geometry relaxations on the low-symmetry structures, which were consistent with X1-P1, X2-P1 and X5-P2 distortions. All of these, however, reverted back to the original γ'-Fe_4N structure. It is possible that there exists a more stable phase of Fe_4N at 30 GPa that is consistent with distortions on a non-linear supercell (more than one active k-point), but these were not investigated here.

VI. RESULTS DISCUSSION

From the energy versus volume graph in Figure 8, it is clear that at both 10 GPa and 30 GPa the P2/m-Fe_4N structure is lower in energy and is thus thermodynamically favoured over the Pm$\bar{3}$m-Fe_4N structure (see data points labelled in black). As shown on the graph the energy difference between the P2/m and Pm$\bar{3}$m structures is more pronounced at 10 GPa than at a pressure of 30 GPa.

In the pressure range 0-4 GPa the Pm$\bar{3}$m structure is lower in energy and is thus thermodynamically favoured over the P2/m structure in this pressure range. Above 4 GPa the P2/m structure becomes more energetically favourable; it remains lower in energy than the Pm$\bar{3}$m structure up to 40 GPa, however the energy difference between the two structures is more pronounced at 10 GPa than at higher pressures.

The results largely agree with the findings of Cheng *et al*, who found the P2/m structure to be more stable than the Pm$\bar{3}$m structure between 2.9 and 19 GPa. Cheng *et al* found the Pm$\bar{3}$m structure to be lower in energy between 1.1 and 2.87 GPa, which is in agreement with

our observations in this pressure range. However, Cheng *et al* found the P2/m structure to be more stable between 0 and 1 GPa, a phenomenon not verified in our study.

V (Å^3)	E_{tot} (Ry)	P (GPa)
54.2048	-1345.31748	-0.053
53.94571	-1345.31742	0.996
53.09991	-1345.31648	3.012
52.61368	-1345.31555	5.052
51.26272	-1345.31151	10.051
50.77519	-1345.30904	11.967
49.6529	-1345.30184	15.984
48.86898	-1345.29536	19.962
47.82894	-1345.28533	24.039
47.21381	-1345.27799	27.964
46.92482	-1345.27414	30.014
46.65458	-1345.27029	32.056
46.1529	-1345.26245	36.049
45.6933	-1345.25443	39.962

FIG. 9: The total energy (E_{tot}) in Ryberg and volume (V) in Å^3 of the P2/m-Fe_4N crystal structure, per formula unit. Results are reported from Quantum Espresso DFT calculations as a function of pressure (P) in GPa.

At each pressure, the P2/m structure was optimized using a 'vc-relax' calculation. In this calculation, a plane wave basis set was defined based on the crystal structure's initial input geometry. The minimum energy structure was found using this plane wave basis set. Upon completion of this geometry optimization, a new plane wave basis set was defined based on the new reciprocal lattice. The energy of the crystal structure is not necessarily minimized for this new plane wave basis set. During this study, a second 'vc-relax' calculation was executed when the final geometry differed significantly from the initial geometry. However, if more 'vc-relax' calculation cycles were implemented, an even lower energy for the P2/m structure would be achieved at each pressure. This could reduce the pressure range over which the $Pm\bar{3}m$ structure is lower in energy then the P2/m structure, which would explain the deviation between those of Cheng *et al*, who observed the $Pm\bar{3}m$ structure to be lower in energy between 1.1 and 2.87 GPa, and the results reported here, where the $Pm\bar{3}m$ structure was found to be lower in energy between 0 and 4 GPa.

The following shortcoming of this study should be noted:

The stability of Fe_4N in the $Pm\bar{3}m$ and P2/m structures at different pressures were compared based on their total energy. The total energy of the $Pm\bar{3}m$ at different pressures was found by changing the length of the cubic unit cell and executing a self-consistent field calculation. No value for the enthalpy of the $Pm\bar{3}m$ crystal structure was obtained from these self-consistent field calculations, and it was thus not possible to compare the enthalpies of the two crystal structures, which would allow for a fairer comparison of the stability of the two structures at non-zero pressures.

[1] P. H. Emmett, S. B. Hendricks, and S. Brunauer, The dissociation pressure of fe_4n, J. Am. Chem. Soc. **52**, 1456 (1930).

[2] F. Yu, H. Zhou, Z. Zhu, J. Sun, R. He, J. Bao, S. Chen, and Z. Ren, Three-dimensional nanoporous iron nitride film as an efficient electrocatalyst for water oxidation, ACS Catal. **7**, 2052–2057 (2017).

[3] J. D. Coey, *Magnetism and Magnetic materials* (Cambridge University Press, 2010).

[4] T. Cheng, G. Yu, Y. Su, L. Zhu, and L. Li, Spontaneous magnetization-induced phonons stability in -fe4n crystalline alloys and high-pressure new phase, J. Magn. Magn. Mater. **451**, 87 (2018).

[5] J. M. D. Coey and P. A. I. Smith, Magnetic nitrides, J. Magn. Magn. Mater. **200**, 405 (1999).

[6] K. Parlinski and Y. Kawazoe1, Ab initio study of phonons and structural stabilities of the perovskite-type $mgsio_3$, Eur. Phys. J. B **16**, 49 (1999).

[7] P. Giannozzi *et al.*, Quantum espresso: a modular and open-source software project for quantum simulations of materials, Journal of Physics: Condensed Matter **21**, 395502 (19pp) (2009).

[8] J. Hook and H. Hall, *Solid State Physics*, Manchester Physics Series (Wiley, 2013).

[9] H. T. Stokes, D. M. Hatch, and B. J. Campbell, Isodisplace: An internet tool for exploring structural distortions., J. Appl. Cryst. **39**, 607 (2006).

[10] H. T. Stokes, D. M. Hatch, and B. J. Campbell, Isodistort, isotropy software suite, iso.byu.edu.